ADVANCED ELECTRONIC MATERIALS
www.advelectronicmat.de

(9,8) Single-Walled Carbon Nanotube Enrichment via Aqueous Two-Phase Separation and Their Thin-Film Transistor Applications

Li Wei, Bilu Liu, Xintian Wang, Hui Gui, Yang Yuan, Shengli Zhai, Andrew Keong Ng, Chongwu Zhou, and Yuan Chen**

Moore's law, which projects the doubling of components on a chip every 18 months, has driven the rapid development of microelectronics industry since 1965. However, from early 2000s, transistor technology based on silicon complementary metal-oxide semiconductor (CMOS) technology has faced more and more technological difficulties in continuously scaling down transistor dimension without performance degradation. This opens the door of developing new transistor materials.[1] Single-walled carbon nanotubes (SWCNTs) have ultrathin body with one atomic phase of graphene wrapped in ≈1 nm diameter cylinder, ballistic transport properties, and intrinsic band gaps.[2] SWCNT transistors have drawn great interests as a potential disruptive force in the electronics industry with a recent demonstration of a functional SWCNT computer.[3] Despite their great promises, a number of challenges remain unsolved. One of the key challenges is to obtain SWCNTs with well-defined structures and properties.

The structure of an SWCNT is defined by a pair of chiral index (n,m). SWCNTs can be conceptually formed by rolling up a graphene sheet along a chiral vector $\boldsymbol{R} = n\boldsymbol{a}_1 + m\boldsymbol{a}_2$ (see Figure S1, Supporting Information). The (n,m) SWCNT has a diameter of d and chiral angle of θ, which could be calculated by

$$d = 0.0783\sqrt{(n^2 + m^2 + nm)} \quad (1)$$

$$\theta = \tan^{-1}\left(\sqrt{3}m / (2n + m)\right) \quad (2)$$

When the (n,m) index satisfies n–m = 3j, where j is an integer, the SWCNT is metallic. In contrast, the SWCNT is semiconducting when n–m = 3j + 1 or 3j + 2. The band gaps of semiconducting SWCNTs are inversely proportional to their diameters. Several SWCNT characteristics are important for transistor applications: (1) SWCNT transistors containing metallic nanotubes may not turn off, leading to shorted devices. Thus, high purity semiconducting SWCNTs are desirable. (2) The diameters of SWCNTs (i.e., specific band gaps) affect their source–drain tunneling and on-state resistance.[4] Some studies have suggested that the optimum diameter range of SWCNTs for transistor applications would lie from about 1.2 to 1.7–2 nm.[1] (3) The diameter distribution of SWCNTs influences the threshold voltage of individual transistors on a chip. Thus, SWCNTs with narrow diameter distribution in the optimum diameter range will have less performance variations among individual transistors.

Commonly available SWCNT samples are mixtures of both metallic and semiconducting nanotubes with typical diameters ranging from 0.6 to 2 nm.[5] Significant efforts have been devoted to formulate separation methods that can yield SWCNTs with desired characteristics for transistor applications. It is hoped that SWCNTs can be grown in bulk, separated in solution, and then placed from solution at precise locations on a CMOS-compatible substrate.[1,6] While several approaches managed to obtain SWCNTs of nearly single (n,m) purity, including density gradient ultracentrifugation,[7] chromatography separation of DNA-wrapped SWCNTs,[8] gel-based electrophoresis and column chromatography,[3g,9] and polymer extraction,[4c,10] they have several limitations in terms of (n,m) purity, selectivity, yield, scalability, and cost. Furthermore, most of the existing separation methods exhibit modest (n,m) selectivity toward large-diameter (>1.1 nm) SWCNTs that are desired for transistor applications.

Recently, aqueous two-phase (ATP) separation emerges as an easily accessible, low-cost, and highly scalable method for sorting SWCNTs.[11] It can spontaneously distribute surfactant dispersed or DNA-wrapped SWCNTs into two aqueous polymer phases of different hydrophobicity. Using surfactants with distinctive affinity for SWCNTs, individual (n,m) species were enriched from small-diameter (<1.1 nm) CoMoCAT SWCNTs,[11a] and metallicity-based separation of large-diameter (>1.4 nm) arc-discharged SWCNTs was also demonstrated.[11e] (n,m) selective enrichment of large-diameter metallic nanotubes (>1.1 nm) was shown using a repetitive ATP separation process.[12]

Here, we demonstrated the simultaneous diameter and metallicity enrichment of large-diameter (9,8) SWCNTs via a one-step ATP separation process. As depicted in **Scheme 1**,

Dr. L. Wei, X. Wang, Y. Yuan, S. Zhai, Prof. Y. Chen
School of Chemical and Biomedical Engineering
Nanyang Technological University
62 Nanyang Drive, Singapore 637459, Singapore
E-mail: chenyuan@ntu.edu.sg
Dr. B. Liu, H. Gui, Prof. C. Zhou
Ming Hsieh Department of Electrical Engineering
Viterbi School of Engineering
University of Southern California
Los Angeles, CA 90089-0271, USA
E-mail: chongwuz@usc.edu
Prof. A. K. Ng
Singapore Institute of Technology
10 Dover Drive, Singapore 138683, Singapore

DOI: 10.1002/aelm.201500151

ADVANCED ELECTRONIC MATERIALS
www.advelectronicmat.de

Materials Views
www.MaterialsViews.com

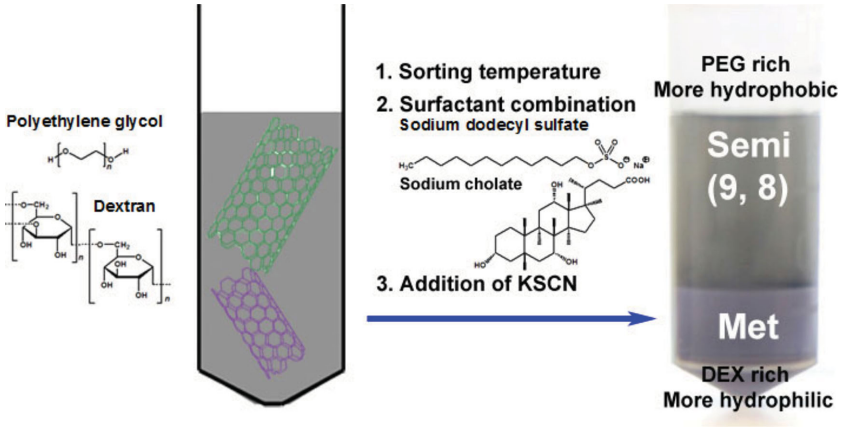

Scheme 1. Schematic illustration of ATP separation for enrichment of (9,8) SWCNTs.

using as-synthesized SWCNTs from $CoSO_4/SiO_2$ catalyst, surfactant dispersed SWCNTs were partitioned in two immiscible aqueous polymer phases formed by polyethylene glycol (PEG) and dextran (DEX). By optimizing separation temperature, the ratio between two surfactants, and addition of a chaotropic salt, we achieved highly efficient enrichment of semiconducting (9,8) SWCNTs in the top PEG phase. The enriched SWCNTs were further used to fabricate thin-film transistors (TFTs), which showed high on/off ratio (up to 10^7) and good motilities (up to 22.34 $cm^2\ V^{-1}\ s^{-1}$). This work shows the excellent potential of using the (9,8)-enriched SWCNTs for transistor applications.

$CoSO_4/SiO_2$ catalyst can be used to synthesize SWCNTs in bulk by chemical vapor deposition (CVD) with carbon monoxide as a carbon precursor (see the Experimental Section for catalyst synthesis and SWCNT growth conditions). The catalyst exhibits unique (n,m) selectivity toward large-diameter semiconducting (9,8) SWCNTs with a diameter of 1.17 nm that are favorable to transistor applications.[1] However, as-synthesized SWCNTs still contain significant amount of small-diameter nanotubes and large-diameter metallic nanotubes. We dispersed the as-synthesized SWCNTs in a 2 wt% sodium cholate (SC) deuterium oxide (D_2O) solution by tip sonication (10 W, 60 min, in ice-water bath) and ultracentrifuge (100 000 *g*, 60 min). The supernatant collected was characterized by photoluminescence (PL) and UV–vis–near-infrared (UV–vis–NIR) absorption spectroscopy. The PL map of the as-synthesized SWCNTs (**Figure 1**a) shows strong signals from small-diameter semiconducting (6,5), (7,5), (7,6), and (8,4) nanotubes. The abundance of (9,8) nanotubes estimated from their PL peak intensity is 29% among all semiconducting nanotubes (see Table S1 in the Supporting Information for the detailed results). It is known that PL spectroscopy is less sensitive toward small chiral angle semiconducting nanotubes due to their lower PL quantum efficiency, and PL spectroscopy can neither detect metallic nanotubes.[13] Therefore, we further analyzed the abundance of different nanotube species using UV–vis–NIR spectroscopy. Figure 1b shows absorption peaks from both semiconducting and metallic nanotubes. Using an electron–phonon interaction model, the UV–vis–NIR spectrum was reconstructed by fitting all (n,m) species using individual Lorentzian peaks (see Table S2 for the detailed calculation method and results, Supporting Information). The major metallic nanotubes identified in the UV–vis–NIR spectrum are (9,6), (9,9), and (10,10) nanotubes. The abundance of all semiconducting nanotubes in as-synthesized SWCNTs is estimated to be 83%, while the abundance of (9,8) nanotubes is 16% among all (n,m) species. For transistor applications, further enrichment of large-diameter semiconducting SWCNTs is desired.

ATP separation can partition nanoparticles by discriminating their surface hydrophobicity into two immiscible polymer phases, which contain polymers of different concentrations. The partition coefficient *K* of an ATP separation may be calculated by the following equation

$$K = \frac{C_t}{C_b} = \exp\left(-\frac{\mu_t^0 - \mu_t^0}{kT}\right) \quad (3)$$

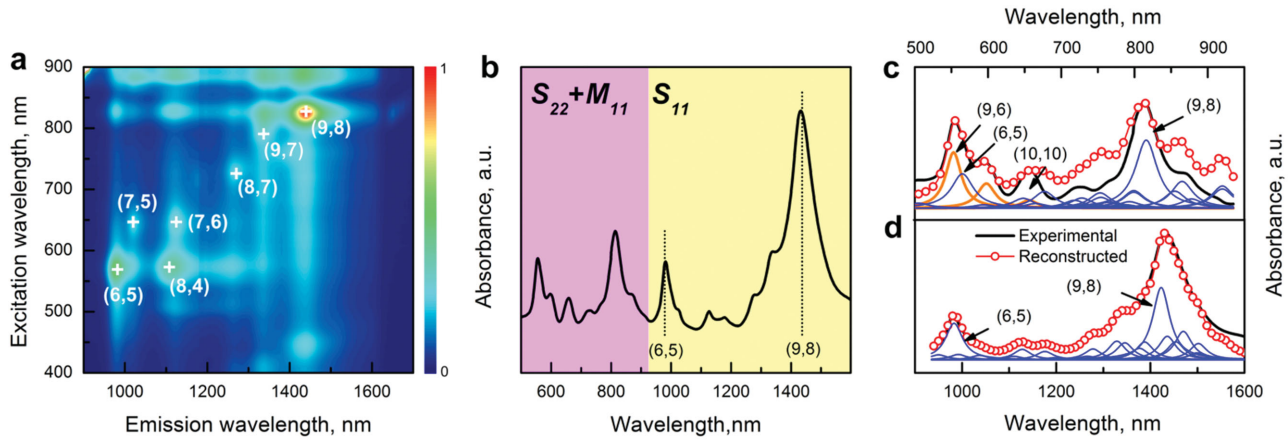

Figure 1. Characterization of as-synthesized SWCNTs from $CoSO_4/SiO_2$ catalyst. a) PL and b) UV–vis–NIR absorption spectrum of nanotube dispersion. Deconvolution of absorption spectrum at c) $S_{22} + M_{11}$ and d) S_{11} regions shows the chirality distribution of (n,m) species.

where C_t, μ^0_t and C_b, μ^0_b are the concentration and standard chemical potential of nanoparticles in the top and bottom phases, respectively. k is the Boltzmann constant, and T is the temperature.[11e] Due to strong internanotube van der Waals force, various amphiphilic surfactants have been used to stabilize individualized SWCNTs by forming micelles on nanotube surface. The surfactant micelles on SWCNT surface display different structures depending on surfactant properties, as well as SWCNT diameter and metallicity. Thus, it is feasible to have diameter and metallicity selective enrichment using ATP separation if the surface hydrophobicity of surfactant wrapped SWCNTs can be carefully tuned. [11d,14] Here, we show that (9,8)-enriched SWCNTs can be obtained in the top PEG phase by optimizing temperature, surfactant combinations, and addition of a salt.

We first established several selection criteria to evaluate the enrichment efficiency at different separation conditions: semiconducting/metallic (semi/met) nanotube ratio (R) and yield of desired nanotubes (Y), i.e., (9,8) nanotubes in this work. The abundance of individual (n,m) species in the two polymer phases can be calculated from the fitted Lorentzian peak areas of their UV–vis–NIR spectra. These abundance data were then used to calculate R and Y (see the Supporting Information for their detailed formula). From experimental data, we found that after separation, a higher semi/met ratio (R) was often coupled with a lower yield (Y) of desired nanotubes in the top PEG phase. Considering that R and Y is a tradeoff in optimizing separation conditions, a figure of merit (F) was defined to assess the overall enrichment efficiency of the ATP separation process

$$F = R \times \left(2 + \log Y\right) \tag{4}$$

The constant "2" was used in Equation (4) because we considered that a separation condition is less useful as a scalable separation process if its yield of desired nanotubes is below 1% (log (0.01) = –2).

As illustrated in Scheme 1, the enrichment of SWCNTs was carried out in a PEG–DEX aqueous mixture (6.3 wt% of both polymers). Surfactant-dispersed SWCNTs were added into the mixture. The PEG–DEX mixture then spontaneously distributed into two phases, including a top hydrophobic PEG-rich phase and a bottom hydrophilic DEX-rich phase. Surfactant-dispersed SWCNTs with different surface hydrophobicity were also partitioned into these two phases. The surfactant combination of sodium dodecyl sulfate (SDS) and SC at the weight ratio of SDS/SC = 3/2 (1.5) was used as the starting condition for optimization, because this surfactant combination has shown some diameter and metallicity selectivity in earlier studies.[14b,15]

As indicated in Equation (3), temperature may have a strong effect on the partition coefficient K. Moreover, the structure of surfactant micelles on SWCNT surface can also be affected by temperature, which alters the value of μ^0.[16] Thus, we optimized the separation temperature first. Photos in Figure S3 (Supporting Information) show that most SWCNTs remain in the hydrophobic top phase at a higher temperature, i.e., 25 °C. When the temperature drops, more SWCNTs gradually move into the hydrophilic bottom phase. Absorption spectra of SWCNTs in the top phase in **Figure 2**a display that the intensity of M_{11} absorption peaks from metallic SWCNTs in the range of 500–700 nm decreases with the declining temperature. These results suggest that surfactant micelles on metallic SWCNTs become more hydrophilic at lower temperature, which help to partition more metallic SWCNTs into the hydrophilic bottom phase while semiconducting nanotube would still reside in the more hydrophobic PEG-rich top phase. Figure 2b confirms that the semi/met ratio (R) increases with the decline of temperature. Although the yield of (9,8) nanotubes (Y) drops slightly (see Table S4, Supporting Information), the overall enrichment efficiency (F) rises from 6.71 to 19.89 when temperature drops from 25 to 5 °C. Thus, the low temperature of 5 °C was chosen as the temperature for further optimization of other experimental parameters.

Although some metallic SWCNTs were portioned into the bottom phase at lower temperature, Figure 2a indicates that the S_{11} absorption peak of small-diameter (6,5) SWCNTs at 976 nm remains unchanged over the entire temperature range from 5 to 25 °C. More small-diameter SWCNTs need to be removed from the top phase. Early studies suggested that SC can selectively disperse smaller diameter SWCNTs as compared to SDS.[11d,14b,15,17] Thus, we optimized the ratio between SDS and SC in an attempt to partition more small-diameter SWCNTs into the bottom phase. Figure 2c shows that the absorption peak intensity of small-diameter (6,5) SWCNTs decreases significantly in compassion to that of large-diameter (9,8) SWCNTs with the reduction of SDS content in the SDS/SC mixture. Moreover, the intensity of absorption peaks from metallic SWCNTs between 500 and 700 nm also decreases with the decrease of SDS content. Figure 2d shows that the semi/met ratio (R) is 17.95 at the SDS/SC ratio of 1.5, and it jumps to 72.65 at the SDS/SC ratio of 0.78. With the increase of SC content in the SDS/SC mixture, not only small-diameter but also more metallic SWCNTs are partitioned into the hydrophilic bottom phase. However, because SC is more hydrophilic than SDS, when the content of SC in the SDS/SC mixture is too high, most of the SWCNTs stay in the hydrophilic bottom phase. The yield of (9,8) SWCNTs (Y) decreases dramatically from 0.128 at the SDS/SC ratio of 1.5 to only 0.032 at the SDS/SC ratio of 0.25. Considering the trade-off between the semi/met ratio and the yield of (9,8) SWCNTs, Figure 2d indicates that the overall enrichment efficiency (F) is at an optimum value of 90.33 when the SDS/SC ratio is 0.78.

Potassium thiocyanate (KSCN), a typical chaotropic salt, can disrupt noncovalent forces in macromolecule dispersions. It has been widely used in ATP separation.[18] Previous studies showed that KSCN can push more nanotubes into the more hydrophilic phase.[11e,19] Although the mechanism behind such a phenomenon is still unclear, it is expected that KSCN may tune surfactant micelle structures around nanotubes, which may enhance the discrimination of various nanotubes according to their diameter and/or metallicity.[20] In this work, KSCN was added intentionally with the hope to further remove metallic and smaller diameter SWCNTs from the top PEG phase. Indeed, as shown in Figure 2e, the absorption peak intensity from both small-diameter and metallic SWCNTs decreases with the increase of KSCN concentration. Figure 2f indicates that the semi/met ratio (R) increases from 72.65 without KSCN to 181.22 at the KSCN concentration of 15×10^{-3} M. However, the yield of (9,8) SWCNTs decreased from 0.175 to 0.024 when KSCN was added. Using the overall

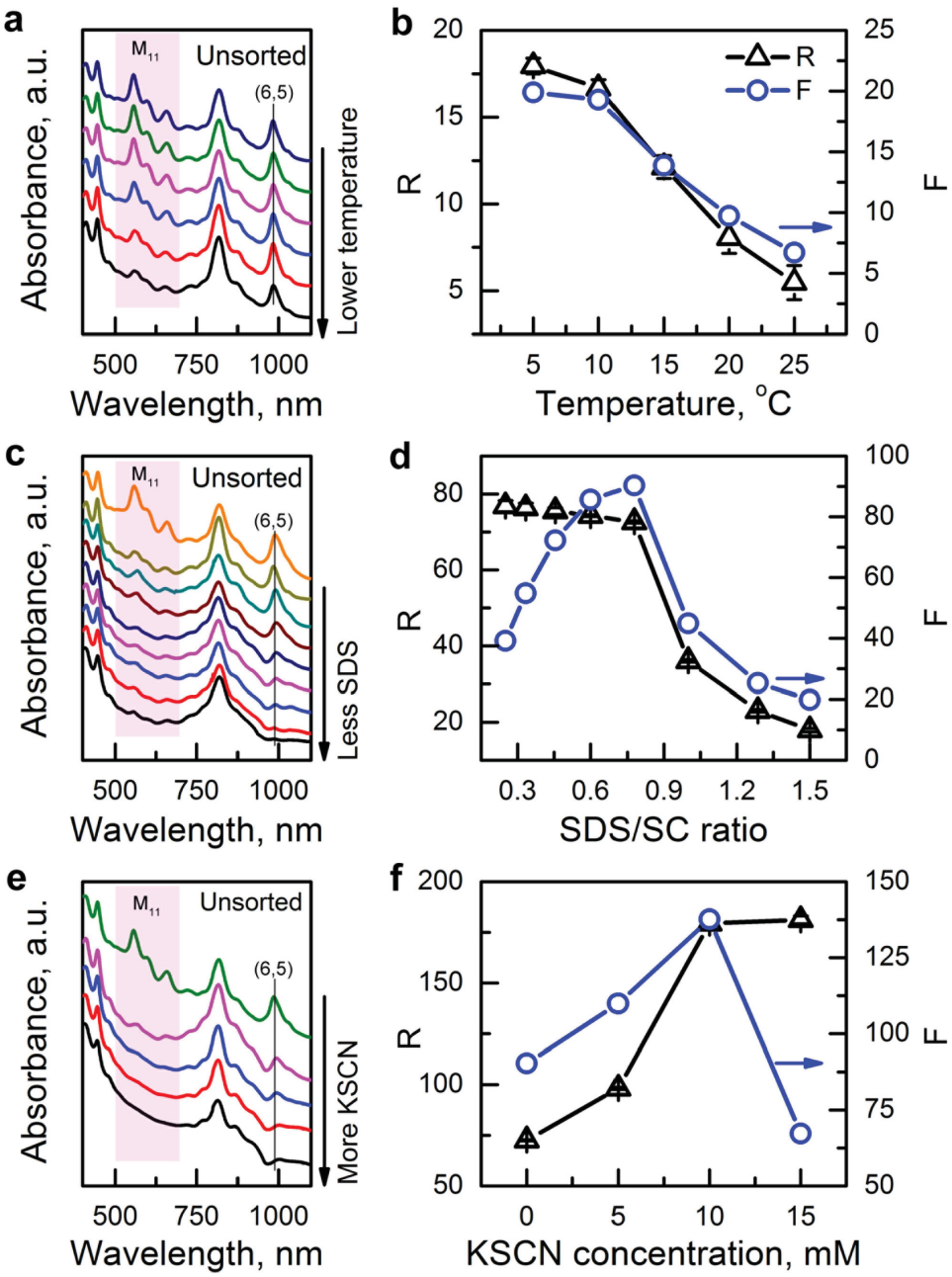

Figure 2. Optimization of the ATP separation process for enriching (9,8) SWCNTs. a,c,e) UV–vis–NIR absorption spectra of SWCNT dispersions in the top phase (PEG enriched) obtained at different separation conditions. b,d,f) Calculated *R* and *F* values at different separation conditions. a,b) Optimization of separation temperature; c,d) optimization of surfactant ratio; and e,f) addition of KSCN.

enrichment efficiency (*F*) as the selection criteria, Figure 2f suggests that the addition of KSCN at the concentration of 10×10^{-3} M achieves the optimum enrichment result. By adding KSCN, more SWCNTs were partitioned into the hydrophilic bottom phase, confirming that KSCN can alter the surfactant micelle structures surrounding nanotubes and make them more hydrophilic. Based on the above experimental results, we speculate that surfactant micelles surrounding metallic and small-diameter nanotubes are more susceptible to KSCN comparing to large-diameter semiconducting nanotubes, resulting in the observed enrichment.

All studied separation parameters are listed in Table S3 (Supporting Information) and their corresponding *R*, *Y*, *F* values are listed in Table S4 (Supporting Information). The optimum enrichment condition for (9,8) SWCNTs is at a low temperature of 5 °C with the surfactant combination of SDS/SC at the ratio of 7/9 and the addition of 10×10^{-3} M KSCN. At this condition, a single-step ATP separation can achieve simultaneous diameter and metallicity enrichment to produce high purity semiconducting SWCNTs enriched with (9,8) nanotubes in the top hydrophobic PEG-rich phase, showing a dark green color; whereas metallic and small-diameter semiconducting SWCNTs

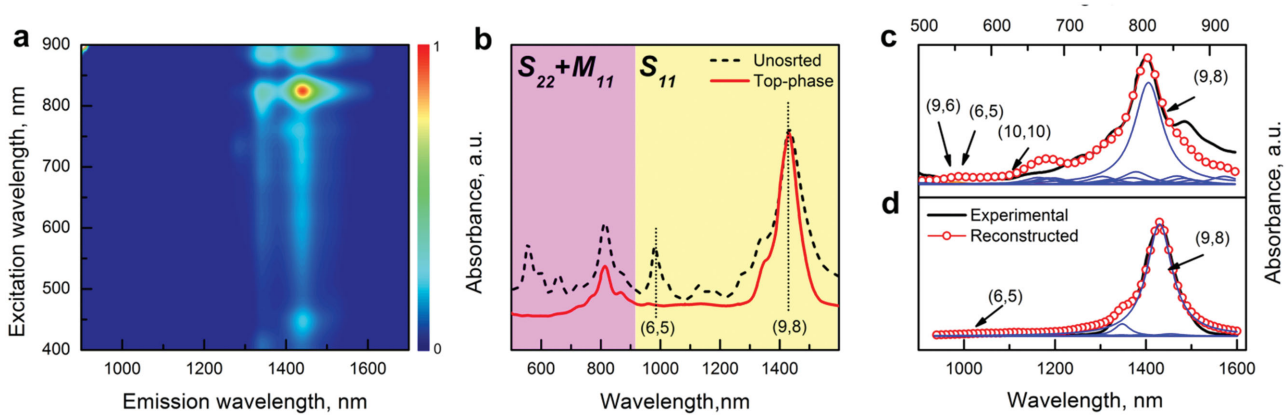

Figure 3. Characterization of enriched SWCNTs in the top PEG phase obtained at the optimal experimental condition. a) PL and b) UV–vis–NIR absorption spectrum. Deconvolution of absorption spectrum at c) $S_{22} + M_{11}$ and d) S_{11} regions shows the chirality distribution of (n,m) species.

reside in the bottom hydrophilic DEX-rich phase, showing a purple color. Enriched SWCNTs from the top phase were redispersed in D_2O for spectroscopic studies. **Figure 3**a shows PL map of the enriched SWCNTs, displaying an intense peak from (9,8) SWCNTs with the absence of peaks from small-diameter semiconducting SWCNTs. The abundance of (9,8) SWCNTs among semiconducting species calculated by their PL intensity is 88.4%. Figure 3b shows that comparing with the unsorted SWCNTs, the features of metallic and small-diameter semiconducting SWCNTs are hardly seen in the UV–vis–NIR spectrum of enriched SWCNTs. The UV–vis–NIR spectrum was reconstructed (Figure 3c) to quantify the abundance of individual (n,m) species. Other than the dominant (9,8) nanotubes, semiconducting large-diameter (9,7) and (10,8) nanotubes were also identified, while metallic species were hardly detected. The abundance of metallic SWCNTs decreases from 16.6% to less than 0.5% with the increase of the semi/met ratio (R) more than 40 times. The abundance of (9,8) SWCNTs among all (n,m) species increases to 84.2%, more than five times compared to that of unsorted SWCNTs. We also analyzed SWCNTs in the bottom phase. Small-diameter semiconducting SWCNTs dominate the PL map (see Figure S4, Supporting Information). Further, higher abundances of metallic SWCNTs were found in the absorption spectrum (see Figure S5, Supporting Information).

To demonstrate the application of (9,8) SWCNTs for TFTs, both unsorted and (9,8)-enriched SWCNTs were deposited on SiO_2/Si wafers (about 15 tubes per μm^2, estimated by atomic force microscope (AFM)) to fabricate back-gated TFTs (see the Experimental Section for fabrication details). Around 25 devices for each SWCNT sample were measured, and their transistor characteristics were compared. The transfer curves ($I_{DS} - V_G$) of unsorted (**Figure 4**a) and enriched (Figure 4c) SWCNT TFTs display unipolar p-type behavior, i.e., the source–drain current, I_{DS}, increases with increasing negative gate voltage. By comparing Figure 4a with Figure 4c, one can clearly discern that unsorted SWCNT devices have metallic behavior, and there are large off-state currents even at the positive gate voltage of 80 V. This finding highlights the existence of significant amount of metallic SWCNTs that form metallic paths in unsorted nanotube devices. On the contrary, the (9,8)-enriched SWCNT devices demonstrate good transistor behaviors, and are fully turned off at a positive gate voltage of 80 V (Figure 4d). The output curves ($I_{DS} - V_{DS}$) of devices fabricated from different samples are shown in the inset of Figure 4a,c. The linear relationship suggests that ohmic contacts are realized in these devices with Ti/Pd electrodes. The statistics of on/off current ratios of SWCNT TFTs are plotted in Figure 4b,d. The I_{DS} values at a gate voltage of −60 V were chosen as the on-state current and the minimum current from the same curve was chosen as the off-state current, and their ratio is defined as the on/off ratio of the device.[21] The on/off ratio of most devices fabricated from (9,8)-enriched SWCNTs fell in the range of 10^5–10^6, which is nearly three-order higher than that of the unsorted SWCNTs (about 10^3). Since the device dimensions are similar, we conclude that the differences of on/off ratios for unsorted and enriched SWCNT TFTs originated from the difference in the amount of metallic nanotubes in these two samples. Therefore, these results show good consistence with the above optical spectroscopic measurements and further demonstrate the effectiveness of the ATP separation process.

Next, we performed more detailed studies on the device performance of (9,8)-enriched SWCNTs with different device dimensions. Normalized on-state current (I_{on}/W) is an important merit for the applications of TFTs, for example, in display electronics. Figure 4e illustrates the relationship between normalized I_{on}/W and device channel length, L. Owing to the formation of more junctions in the channel with increased channel resistance, I_{on}/W decreases as the channel length increases. Specifically, the devices show I_{on}/W of 0.05 μA/μm at a small V_{ds} of 0.1 V, which is comparable with very recent results on SWCNT TFTs.[22] In addition to the on-state current, carrier mobility is another critical parameter for nanotube TFTs, which can be calculated using the following equation

$$\mu_{device} = \frac{L}{V_D C_{ox} W} \frac{dI_d}{dV_g} = \frac{L}{V_D C_{ox}} \frac{g_m}{W} \tag{5}$$

where μ is the mobility of the device, L and W are, respectively, the channel length and channel width of the device, V_d is the source–drain bias, C_{ox} is the gate capacitance, and g_m

ADVANCED ELECTRONIC MATERIALS
www.advelectronicmat.de

Materials Views
www.MaterialsViews.com

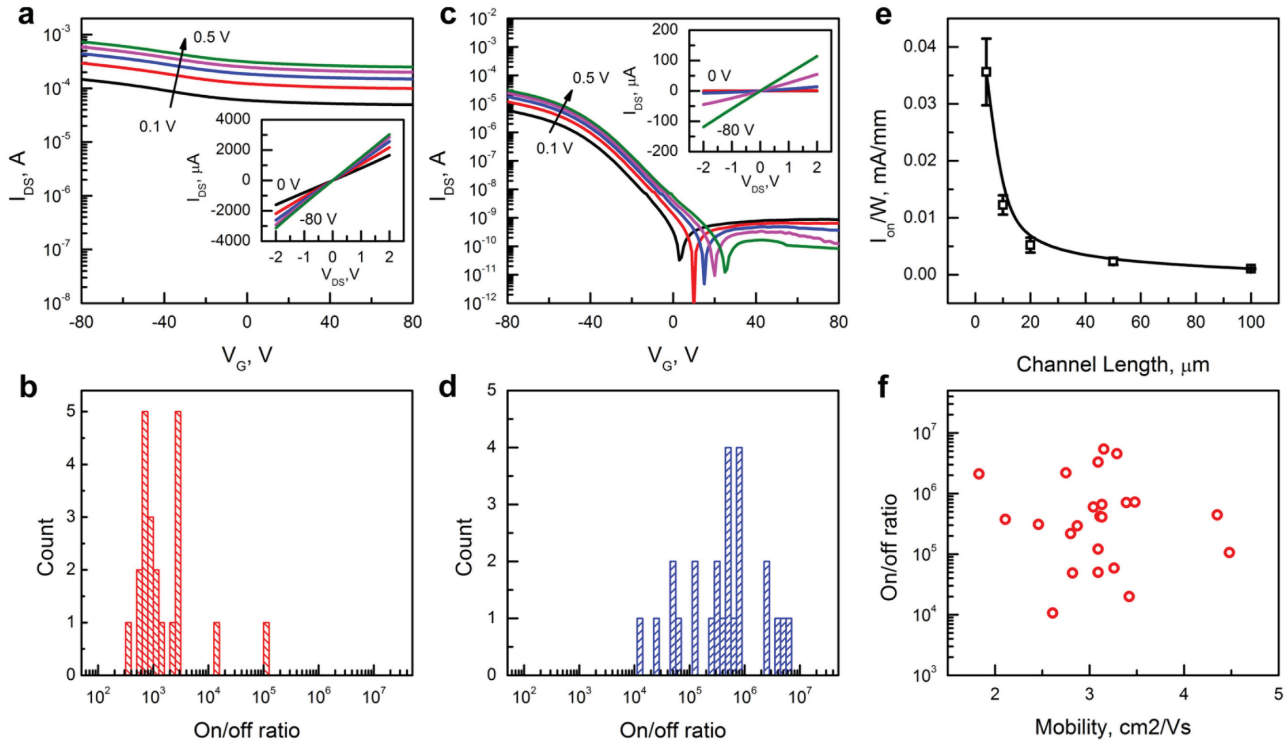

Figure 4. Transfer characteristic curves and statistic histogram of on/off ratios of SWCNT TFTs fabricated from a,b) unsorted and c,d) (9,8)-enriched SWCNTs. e) Normalized I_{on} versus channel length (4, 10, 20, 50, or 100 μm) and f) mobility versus on/off ratio.

is the transconductance of the device, which can be extracted from transfer curves. We found that the average mobility of the TFTs using enriched SWCNTs is 3.08 ± 0.58 $cm^2 V^{-1} s^{-1}$, with the maximum value of 4.48 $cm^2 V^{-1} s^{-1}$. This mobility value is comparable to SWCNT TFTs with similar diameters reported recently,[22] as well as polymer-enriched arc-discharge SWCNTs (diameter at 1.3–1.4 nm).[23] A comparison with recent literature data is given in Table S5 (Supporting Information). We plotted mobility versus on/off ratio for our TFTs in Figure 4f. The results imply that most devices fall in the range of 3–4 $cm^2 V^{-1} s^{-1}$ for mobility and 10^4 to 10^6 for on/off ratio.

Because (9,8)-enriched SWCNTs obtained in this work have high semiconducting purity, the transfer property, i.e., mobility, of fabricated SWCNT TFTs can be further improved by increasing SWCNT density in TFT channels. Thin films of higher SWCNT densities (about 25 and 50 tubes per μm^2) were prepared by drop casting more enriched SWCNT dispersions. The SWCNT films were annealed at 200 °C for 2 h to reduce contact resistance among nanotubes.[24] About 20 devices were measured at each SWCNT density, and their on/off ratio and mobility are presented in **Figure 5**. The device mobility rises with the increase of SWCNT density. The average mobility increases to 10.66 ± 2.03 and 22.34 ± 3.51 for TFTs containing SWCNTs of 25 and 50 tubes per μm^2 in device channel, respectively. More importantly, their on/off ratios show moderate drops. Most of the measured TFTs have the on/off ratio of about 10^5. Overall, these device measurement results indicate that (9,8)-enriched SWCNTs via ATP separation have good performance as channel materials for TFTs.

In summary, we demonstrated simultaneous diameter and metallicity enrichment of large-diameter (9,8) SWCNTs in one separation step from as-synthesized SWCNTs on $CoSO_4$/SiO_2 catalyst using the new ATP separation process. Systematic separation parameter studies showed that the optimum enrichment conditions are (1) separation temperature of 5 °C,

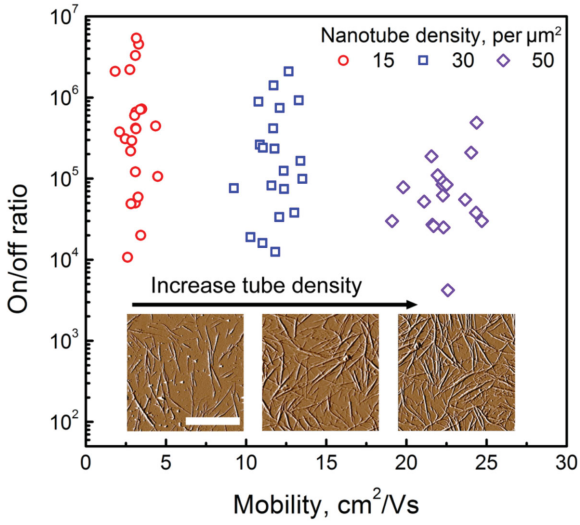

Figure 5. On/off ratio plotted against mobility for SWCNT TFTs with different nanotube densities. Insets show typical AFM images of SWCNT networks in device channels. The scale bar in the AFM images is 1 μm.

(2) SDS/SC surfactant ratio of 7/9, and (3) addition of KSCN at the concentration of 10×10^{-3} M. Under this optimum separation condition, the abundance of (9,8) nanotubes in the top PEG phase increases to 84.2%, and the ratio of semiconducting to metallic increases more than 40 times compared to as-synthesized nanotubes. The enriched (9,8) SWCNTs were used to fabricate TFTs, showing high on/off ratios (up to 10^7). The average device mobility of 3.08 $cm^2 V^{-1} s^{-1}$ was obtained at the SWCNT network density of about 15 tubes per μm^2, and is further increased to 22.34 $cm^2 V^{-1} s^{-1}$ at 50 tubes per μm^2, while the on/off ratio remains around 10^5. These results demonstrate the great potential of using these (9,8)-enriched SWCNTs for transistor applications. Furthermore, the (9,8)-enriched nanotubes with a narrow emission window of around 1400 nm may be useful for many applications in the new generation of optoelectronic devices.

Experimental Section

Synthesis of SWCNTs Using $CoSO_4/SiO_2$ Catalyst: SWCNTs were synthesized by CVD using carbon monoxide on $CoSO_4/SiO_2$ catalyst.[25] The catalyst was prepared by loading 1 wt% Co (from $CoSO_4 \cdot 7H_2O$) on fumed porous SiO_2, followed by calcination at 440 °C in air for 4 h. The growth of SWCNTs was performed in a CVD reactor. About 200 mg of the catalyst was loaded in a ceramic boat and placed in the center of the reactor. After reduction in H_2 (1 atm, 150 mL min^{-1}) from room temperature to 540 °C, the reactor was purged with Ar till its temperature increased to 780 °C. Subsequently, CO at 5 atm was introduced to the reactor at 150 mL min^{-1} for 30 min. After growth, the reactor was cooled to room temperature in flowing Ar. The as-synthesized SWCNTs were further purified by a four-step method reported earlier to remove catalyst residues and other carbon species.[26]

PLE and UV–Vis–NIR Spectroscopic Studies of SWCNTs: Purified SWCNTs were dispersed in 2 wt% SC D_2O (99.9%, Sigma) solution for spectroscopic analysis. ATP separations were performed in aqueous (H_2O) solution. To avoid the interferences from H_2O, polymers and surfactants on UV–vis–NIR absorption data, blank solutions containing the same type and amount of polymers and surfactants without SWCNTs were prepared at each ATP separation condition as references for background subtraction. At the optimal ATP separation condition, enriched SWCNTs were redispersed in 2 wt% SC D_2O solution for spectroscopic analysis. UV–vis–NIR absorption spectra of SWCNT dispersions were collected on a UV–vis–NIR spectrometer (Varian Cary 5000) with a 0.5 nm step in a 10 mm light path quartz cuvette. PL maps were collected on a PL spectrometer (Horiba/Jobin Yvon Nanolog-3) with a 350 W Xenon lamp as the excitation light source. A step of 2 nm was chosen for excitation light.

ATP Separation: SWCNTs were first dispersed in 2 wt% SC aqueous solution by tip sonication (10 W, VCX-130, Vibracell) in an ice-water bath for 1 h. After centrifugation at 100 000 *g* for 1 h, the upper 60% of SWCNT dispersion was collected for ATP separation. Several stock solutions were prepared to create different separation conditions. PEG (50 wt%, 6 kDa, Alfa-Aesar) and DEX (20 wt%, 150 kDa, Sigma) aqueous solutions were prepared by dissolving polymer powders in deionized water under shaking at 300 rpm overnight. Two surfactant solutions (10 wt%), SDS and SC, were prepared to dissolve surfactants in deionized water. KSCN was dissolved in deionized water at 1 M. The total surfactant concentration was kept at 1.6 wt% for all ATP conditions. This concentration was used for two reasons. First, a previous study suggested the optimal window of total surfactant concentration for semi/metallic SWCNT separation should be greater than 1.2 wt%.[11e] Second, the critical micelle concentration of SDS is 8.2×10^{-3} M (0.24 wt%) at 25 °C,[27] and that of SC is 14×10^{-3} M (0.63 wt%) at 25 °C.[28] Thus, The total concentration of 1.6 wt% is sufficient to form micelles for at least one type of surfactants in different surfactant combinations used in this study. At a typical separation condition, 0.3 mL DEX solution and 0.12 mL PEG solution were first mixed in a 1.5 mL centrifugation tube. SC and SDS stock solutions were then added with different combinations to create various ATP conditions. Subsequently, appropriate amount of water and/or KSCN solution was added to increase the total liquid volume of 0.82 mL. Afterward, 0.2 mL of SWCNT dispersion was added. The detailed compositions are listed in Table S3 (Supporting Information). The dispersion was mixed by vortex for 30 s before it was placed in a water bath for 5 min at different temperatures. To enhance temperature uniformity in the dispersion, the mixture was further mixed by vortex for 30 s, followed by incubation in the water bath for another 15 min. Then, the dispersion was centrifuged at 2 600 *g* for 5 min to speed up its partition into two phases with different colors. Last, the two phases were extracted for spectroscopic analysis.

Fabrication and Characterization of SWCNT TFTs: To remove polymers from enriched SWCNT dispersions, additional KSCN was added at a concentration of 0.1 M. The mixtures were kept at 4 °C in a refrigerator overnight, which allows SWCNTs to agglomerate together. SWCNT agglomerates were then collected by centrifuge and washed using deionized water. The recovered SWCNTs were dispersed in 2 wt% SC solution by tip sonication at 20 W in an ice-water bath for 30 min, followed by centrifugation at 50 000 *g* for 1 h. The dispersion was then used to create SWCNT networks on SiO_2/Si substrates (the thickness of SiO_2 is 300 nm). Before SWCNT deposition, SiO_2/Si substrates were first pretreated with 0.5 wt% poly(L-lysine) aqueous solution (Sigma) for 5 min, followed by incubation in SWCNT solution for 10 min. Two methods were used to fabricate SWCNT TFTs. First, in order to make a quick evaluation of the semiconducting nanotube purity, back gated nanotube devices with different dimensions were fabricated using photolithograph. The channel lengths are 4, 10, 20, 50, or 100 μm, and channel widths are 200, 400, 800, 1200, 1600, or 2000 μm. The contact metal was Ti/Pd with a thickness of 0.5 nm/50 nm, and was deposited using e-beam evaporator. Second, in order to further increase SWCNT density in TFT channels, enriched SWCNT dispersion in device channels of prefabricated TFTs was further dropped, which were fabricated by photolithograph with Ti/Pd metal electrode (thickness of 0.5 nm/50 nm); channel width is 200 μm and the length is 50 μm. The dropped SWCNT films were washed with DI water and methanol. This drop casting process was repeated several times until the desired SWCNT density was obtained. SWCNT networks were imaged by AFM (MFP3D) in AC mode. The transport performance of fabricated SWCNT TFTs was collected using a semiconductor parameter analyzer (Agilent 4156B) under ambient conditions.

Supporting Information

Supporting Information is available from the Wiley Online Library or from the author.

Acknowledgements

This work was supported by the Ministry of Education, Singapore (MOE2011-T2-2-062 and 2013-T1-002-132) and iFood program funded by Nanyang Technological University.

Received: May 5, 2015
Revised: September 1, 2015
Published online:

[1] G. S. Tulevski, A. D. Franklin, D. Frank, J. M. Lobez, Q. Cao, H. Park, A. Afzali, S. J. Han, J. B. Hannon, W. Haensch, *ACS Nano* **2014**, *8*, 8730.
[2] A. Javey, J. Guo, Q. Wang, M. Lundstrom, H. Dai, *Nature* **2003**, *424*, 654.
[3] a) M. Steiner, M. Engel, Y.-M. Lin, Y. Wu, K. Jenkins, D. B. Farmer, J. J. Humes, N. L. Yoder, J.-W. T. Seo, A. A. Green, M. C. Hersam, R. Krupke, P. Avouris, *Appl. Phys. Lett.* **2012**, *101*, 053123;

b) E. L. Gui, L.-J. Li, K. Zhang, Y. Xu, X. Dong, X. Ho, P. S. Lee, J. Kasim, Z. X. Shen, J. A. Rogers, Mhaisalkar, *J. Am. Chem. Soc.* **2007**, *129*, 14427; c) P. H. Lau, K. Takei, C. Wang, Y. Ju, J. Kim, Z. Yu, T. Takahashi, G. Cho, A. Javey, *Nano Lett.* **2013**, *13*, 3864; d) D. Kiriya, K. Chen, H. Ota, Y. Lin, P. Zhao, Z. Yu, T.-j. Ha, A. Javey, *J. Am. Chem. Soc.* **2014**, *136*, 11188; e) A. Bachtold, P. Hadley, T. Nakanishi, C. Dekker, *Science* **2001**, *294*, 1317; f) M. M. Shulaker, G. Hills, N. Patil, H. Wei, H.-Y. Chen, H. S. P. Wong, S. Mitra, *Nature* **2013**, *501*, 526; g) S.-J. Choi, P. Bennett, K. Takei, C. Wang, C. C. Lo, A. Javey, J. Bokor, *ACS Nano* **2013**, *7*, 798.

[4] a) Z. Chen, J. Appenzeller, J. Knoch, Y.-m. Lin, P. Avouris, *Nano Lett.* **2005**, *5*, 1497; b) M. Ganzhorn, A. Vijayaraghavan, S. Dehm, F. Hennrich, A. A. Green, M. Fichtner, A. Voigt, M. Rapp, H. von Löhneysen, M. C. Hersam, M. M. Kappes, R. Krupke, *ACS Nano* **2011**, *5*, 1670; c) D.-M. Sun, C. Liu, W.-C. Ren, H.-M. Cheng, *Small* **2013**, *9*, 1188; d) M. F. L. De Volder, S. H. Tawfick, R. H. Baughman, A. J. Hart, *Science* **2013**, *339*, 535; e) B. Liu, C. Wang, J. Liu, Y. Che, C. Zhou, *Nanoscale* **2013**, *5*, 9483.

[5] H. Wang, Y. Yuan, L. Wei, K. Goh, D. Yu, Y. Chen, *Carbon* **2015**, *81*, 1.

[6] R. H. Baughman, A. A. Zakhidov, W. A. de Heer, *Science* **2002**, *297*, 787.

[7] a) M. S. Arnold, A. A. Green, J. F. Hulvat, S. I. Stupp, M. C. Hersam, *Nat. Nanotechnol.* **2006**, *1*, 60; b) S. Ghosh, S. M. Bachilo, R. B. Weisman, *Nat. Nanotechnol.* **2010**, *5*, 443.

[8] a) M. Zheng, E. D. Semke, *J. Am. Chem. Soc.* **2007**, *129*, 6084; b) X. M. Tu, S. Manohar, A. Jagota, M. Zheng, *Nature* **2009**, *460*, 250.

[9] a) S. Diao, G. S. Hong, J. T. Robinson, L. Y. Jiao, A. L. Antaris, J. Z. Wu, C. L. Choi, H. J. Dai, *J. Am. Chem. Soc.* **2012**, *134*, 16971; b) J. Liu, C. Wang, X. Tu, B. Liu, L. Chen, M. Zheng, C. Zhou, *Nat. Commun.* **2012**, *3*, 1199; c) M. Engel, J. P. Small, M. Steiner, M. Freitag, A. A. Green, M. C. Hersam, P. Avouris, *ACS Nano* **2008**, *2*, 2445; d) B. S. Flavel, M. M. Kappes, R. Krupke, F. Hennrich, *ACS Nano* **2013**, *7*, 3557.

[10] a) F. Chen, B. Wang, Y. Chen, L.-J. Li, *Nano Lett.* **2007**, *7*, 3013; b) A. Nish, J. Y. Hwang, J. Doig, R. J. Nicholas, *Nat. Nanotechnol.* **2007**, *2*, 640; c) G. Liu, A. F. M. M. Rahman, S. Chaunchaiyakul, T. Kimura, Y. Kuwahara, N. Komatsu, *Chem. Eur. J.* **2013**, *19*, 16221; d) G. Liu, Y. Saito, D. Nishio-Hamane, A. K. Bauri, E. Flahaut, T. Kimura, N. Komatsu, *J. Mater. Chem. A* **2014**, *2*, 19067; e) R. Si, L. Wei, H. Wang, D. Su, S. H. Mushrif, Y. Chen, *Chem. Asian J.* **2014**, *9*, 868.

[11] a) J. A. Fagan, C. Y. Khripin, C. A. Silvera Batista, J. R. Simpson, E. H. Hároz, A. R. Hight Walker, M. Zheng, *Adv. Mater.* **2014**, *26*, 2800; b) M. Zhang, C. Y. Khripin, J. A. Fagan, P. McPhie, Y. Ito, M. Zheng, *Anal. Chem.* **2014**, *86*, 3980; c) H. Gui, J. K. Streit, J. A. Fagan, A. R. Hight Walker, C. Zhou, M. Zheng, *Nano Lett.* **2015**; d) N. K. Subbaiyan, S. Cambré, A. N. G. Parra-Vasquez, E. H. Hároz, S. K. Doorn, J. G. Duque, *ACS Nano* **2014**, *8*, 1619; e) C. Y. Khripin, J. A. Fagan, M. Zheng, *J. Am. Chem. Soc.* **2013**, *135*, 6822.

[12] J. A. Fagan, E. H. Haroz, R. Ihly, H. Gui, J. L. Blackburn, J. R. Simpson, S. Lam, A. R. Hight Walker, S. K. Doorn, M. Zheng, *ACS Nano* **2015**, *9*, 5377.

[13] Y. Oyama, R. Saito, K. Sato, J. Jiang, G. G. Samsonidze, A. Grüneis, Y. Miyauchi, S. Maruyama, A. Jorio, G. Dresselhaus, M. S. Dresselhaus, *Carbon* **2006**, *44*, 873.

[14] a) H. Wang, W. Zhou, D. L. Ho, K. I. Winey, J. E. Fischer, C. J. Glinka, E. K. Hobbie, *Nano Lett.* **2004**, *4*, 1789; b) L. Wei, B. Wang, T. H. Goh, L.-J. Li, Y. Yang, M. B. Chan-Park, Y. Chen, *J. Phys. Chem. B* **2008**, *112*, 2771; c) M. S. Arnold, A. A. Green, J. F. Hulvat, S. I. Stupp, M. C. Hersam, *Nat. Nanotechnol.* **2006**, *1*, 60; d) E. J. F. Carvalho, M. C. dos Santos, *ACS Nano* **2010**, *4*, 765.

[15] L. Wei, C. W. Lee, L.-J. Li, H. G. Sudibya, B. Wang, L. Q. Chen, P. Chen, Y. Yang, M. B. Chan-Park, Y. Chen, *Chem. Mater.* **2008**, *20*, 7417.

[16] S. Niyogi, C. G. Densmore, S. K. Doorn, *J. Am. Chem. Soc.* **2009**, *131*, 1144.

[17] T. J. McDonald, C. Engtrakul, M. Jones, G. Rumbles, M. J. Heben, *J. Phys. Chem. B* **2006**, *110*, 25339.

[18] B. Y. Zaslavsky, *Aqueous Two-Phase Partitioning: Physical Chemistry and Bioanalytical Applications*, M. Dekker, New York **1995**.

[19] G. Ao, C. Y. Khripin, M. Zheng, *J. Am. Chem. Soc.* **2014**, *136*, 10383.

[20] P. Lo Nostro, B. W. Ninham, *Chem. Rev.* **2012**, *112*, 2286.

[21] M. Timmermans, D. Estrada, A. Nasibulin, J. Wood, A. Behnam, D.-m. Sun, Y. Ohno, J. Lyding, A. Hassanien, E. Pop, E. Kauppinen, *Nano Res.* **2012**, *5*, 307.

[22] J. Zhang, H. Gui, B. Liu, J. Liu, C. Zhou, *Nano Res.* **2013**, *6*, 906.

[23] H. Wang, J. Mei, P. Liu, K. Schmidt, G. Jiménez-Osés, S. Osuna, L. Fang, C. J. Tassone, A. P. Zoombelt, A. N. Sokolov, K. N. Houk, M. F. Toney, Z. Bao, *ACS Nano* **2013**, *7*, 2659.

[24] A. Vijayaraghavan, S. Blatt, D. Weissenberger, M. Oron-Carl, F. Hennrich, D. Gerthsen, H. Hahn, R. Krupke, *Nano Lett.* **2007**, *7*, 1556.

[25] H. Wang, L. Wei, F. Ren, Q. Wang, L. D. Pfefferle, G. L. Haller, Y. Chen, *ACS Nano* **2012**, *7*, 614.

[26] Y. Chen, L. Wei, B. Wang, S. Lim, D. Ciuparu, M. Zheng, J. Chen, C. Zoican, Y. Yang, G. L. Haller, L. D. Pfefferle, *ACS Nano* **2007**, *1*, 327.

[27] A. Cifuentes, J. L. Bernal, J. C. Diez-Masa, *Anal. Chem.* **1997**, *69*, 4271.

[28] C. M. Hebling, L. E. Thompson, K. W. Eckenroad, G. A. Manley, R. A. Fry, K. T. Mueller, T. G. Strein, D. Rovnyak, *Langmuir* **2008**, *24*, 13866.